Inorganic Chemistry

Article

pubs.acs.org/IC

Unexpected Direct Reduction Mechanism for Hydrogenation of Ketones Catalyzed by Iron PNP Pincer Complexes

Xinzheng Yang*

Molecular Graphics and Computation Facility, College of Chemistry, University of California, Berkeley, California 94720, United States

Supporting Information

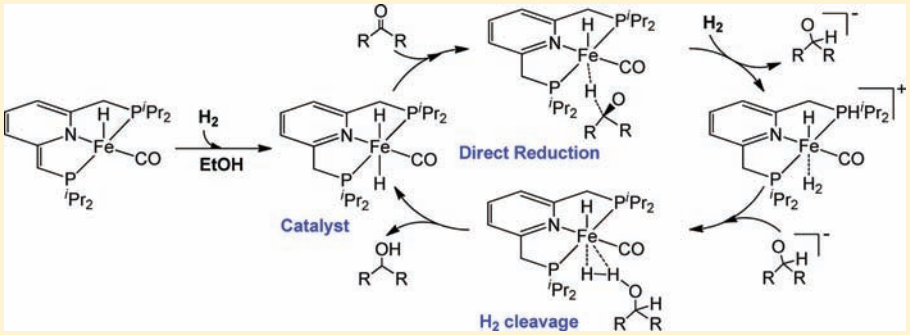

ABSTRACT: The hydrogenation of ketones catalyzed by 2,6-bis(diisopropylphosphinomethyl)pyridine (PNP)-ligated iron pincer complexes was studied using the range-separated and dispersion-corrected ωB97X-D functional in conjunction with the all-electron 6-31++G(d,p) basis set. A validated structural model in which the experimental isopropyl groups were replaced with methyl groups was employed for the computational study. Using this simplified model, the calculated total free energy barrier of a previously postulated mechanism with the insertion of ketone into the Fe−H bond is far too high to account for the observed catalytic reaction. Calculation results reveal that the solvent alcohol is not only a stabilizer of the dearomatized intermediate but also more importantly an assistant catalyst for the formation of *trans*-(PNP)Fe(H)$_2$(CO), the actual catalyst for hydrogenation of ketones. A direct reduction mechanism, which features the solvent-assisted formation of a *trans* dihydride complex *trans*-(PNP)Fe(H)$_2$(CO), direct transfer of hydride to acetophenone from *trans*-(PNP)Fe(H)$_2$(CO) for the formation of a hydrido alkoxo complex, and direct H_2 cleavage by hydrido alkoxo without the participation of the pincer ligand for the regeneration of *trans*-(PNP)Fe(H)$_2$(CO), was predicted.

INTRODUCTION

The catalytic hydrogenation of ketones is an important reaction for the production of enantiopure alcohols in fine chemical and pharmaceutical industries.[1] Although considerable progress has been achieved in transition metal-catalyzed hydrogenation and transfer hydrogenation of ketones, most of the reported high-efficiency catalysts contain noble metals like ruthenium, rhodium, iridium, etc.[2] Scarcity, cost, and toxicity are major factors preventing the large-scale application of noble metal catalysts and driving the efforts to develop alternative base metal catalysts. A few recently reported base metal hydrogenation catalysts either require high-pressure H_2 or have quite low turnover frequencies (TOFs).[3] The design of high-efficiency, low-cost, and environmentally benign iron-based catalysts for the reduction of ketones is therefore strongly desired.

Very recently, Milstein and co-workers[4] developed an iron pincer complex (PNP)FeH(CO)Br [**1**; PNP is 2,6-bis-(diisopropylphosphinomethyl)pyridine], which is the most efficient iron-based catalyst so far for hydrogenation of ketones under mild conditions. The TOF of the hydrogenation of acetophenone catalyzed by **1** is 87 h^{-1} at room temperature with only 4.1 atm of H_2. A postulated catalytic cycle (Scheme 1) containing a dearomatized intermediate (**2**), coordination of ketones to the position *cis* to the hydride (**3**), the insertion of the ketones into the Fe−H bond (**4**), the H_2 splitting for the rearomatization of the PNP ligand (**5**), and proton transfer for the formation of an O−H bond in alcohols was proposed. Because the observed catalytic ketone hydrogenation reaction could happen only in alcoholic solvents, the ethanol molecule was considered as a stabilizer of **2** with reversible formation of a more stable intermediate **6** in the proposed catalytic mechanism. However, the formation of a *trans*-dihydride complex *trans*-(PNP)Fe(H)$_2$(CO) (**7**), which was also observed by Milstein and co-workers in their experiments, was not considered in the proposed mechanism. It is worth noting that **7** was computationally predicted as an efficient catalyst for hydrogenation of carbon dioxide by Yang[5] and then experimentally confirmed as the most efficient iron catalyst so

Received: September 14, 2011
Published: November 21, 2011

Scheme 1. The Previously Postulated Catalytic Mechanism of Milstein (red, R = ^{i}Pr) Did Not Consider the Formation of Stable Complexes 7 (blue) and 3′ (purple, an isomer of 3)

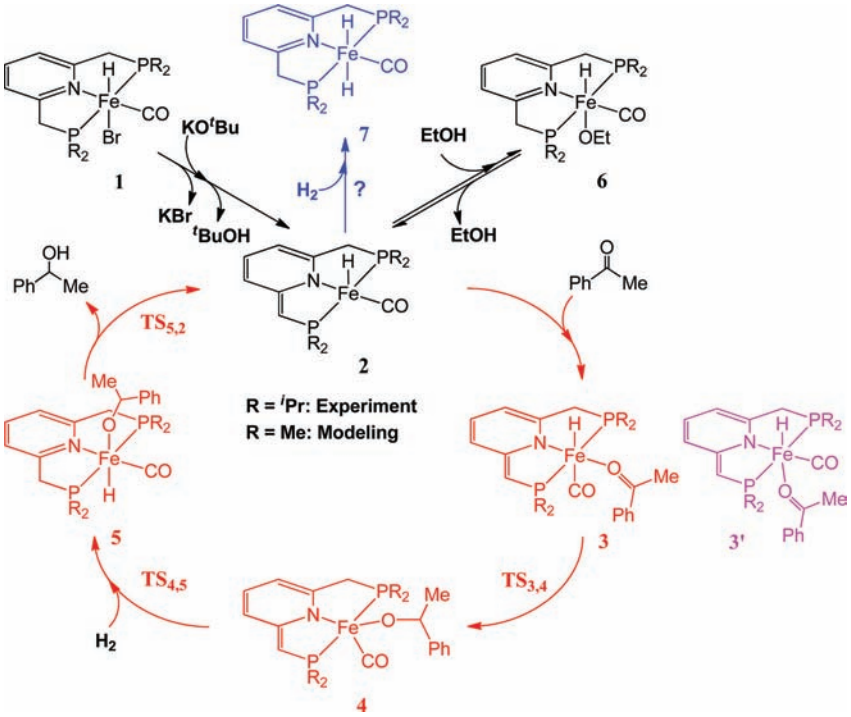

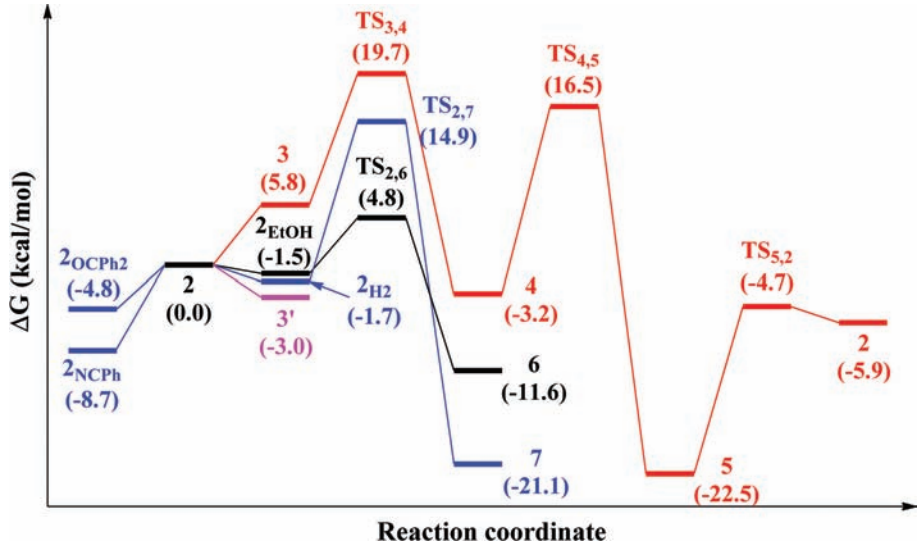

Figure 1. Calculated relative free energies in the ketone insertion mechanism (red), the reversible addition of EtOH (black), the formation of **7** by direct H_2 cleavage (blue), and the formation of **3′** (purple).

far for low-pressure hydrogenation of carbon dioxide by Milstein and co-workers.[6]

In this Article, the hydrogenation of acetophenone catalyzed by iron PNP pincer complexes was studied using density functional theory (DFT).[7] A simplified structural model, in which the experimental isopropyl groups were replaced with methyl groups, was employed for computational study. Detailed evaluations of density functionals and the structural model are provided in Computational Details. The catalytic cycle proposed by Milstein and co-workers was examined computationally using this simplified model. The essential role of solvent ethanol in the reaction was analyzed with the finding of a low-barrier pathway for the formation of **7**. Finally, an unexpected direct reduction mechanism for the hydrogenation of ketones catalyzed by **7** was discovered on the basis of DFT calculations.

RESULTS AND DISCUSSION

Ketone Insertion Mechanism. Because the hydrido bromide complex **1** reacts with KO^{t}Bu immediately in the solvent and **1** is not in the catalytic cycle, the dearomatized intermediate **2** (Figure 1) is therefore set as the zero point of the calculated free energy profile. Depending on which molecule (acetophenone, EtOH, or H_2) coordinates to **2**, there are three possible reactions. In the catalytic cycle proposed by Milstein and co-workers (red), a postulated

dx.doi.org/10.1021/ic2020176 | *Inorg. Chem.* 2011, 50, 12836–12843

intermediate **3** (Figure 2) is formed by coordinating an acetophenone molecule to the iron center at the position *trans*

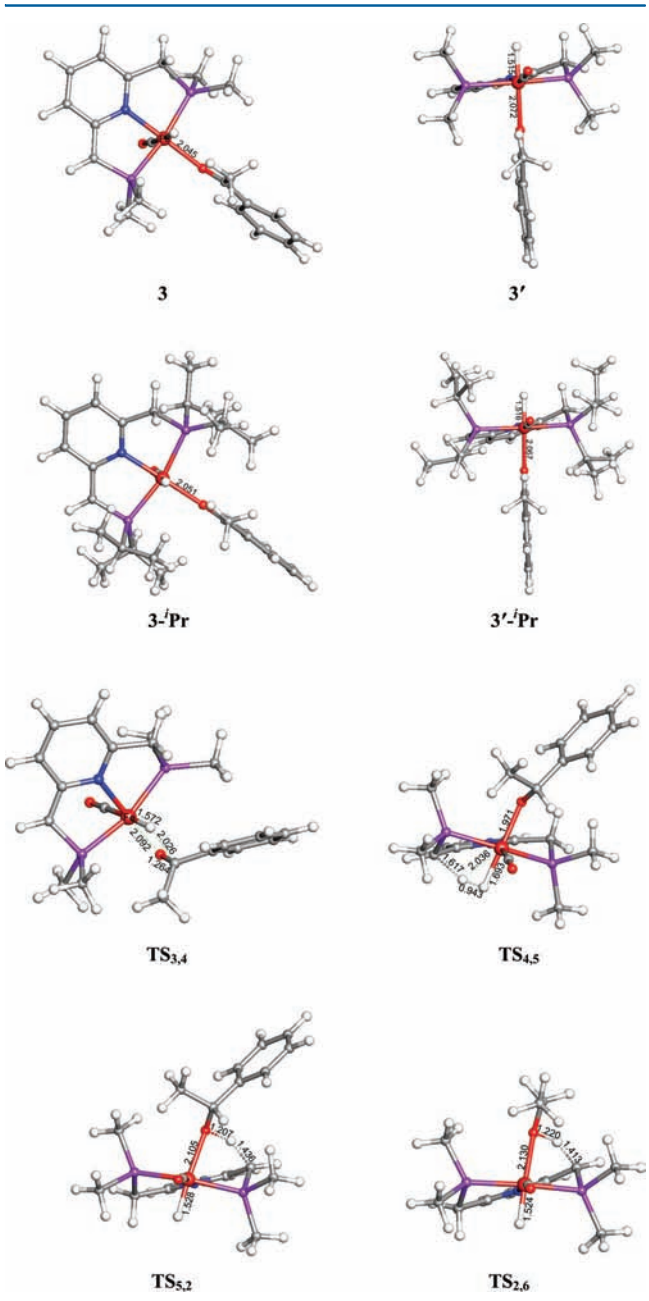

Figure 2. Optimized structures of **3**, **3′**, **3**-^{i}**Pr**, **3′**-^{i}**Pr**, $\mathbf{TS}_{3,4}$ (179*i* cm^{-1}), $\mathbf{TS}_{4,5}$ (1209*i* cm^{-1}), $\mathbf{TS}_{5,2}$ (1408*i* cm^{-1}), and $\mathbf{TS}_{2,6}$ (1418*i* cm^{-1}). Bond lengths are in angstroms.

to the nitrogen atom with an Fe−O distance of 2.045 Å. The carbonyl is rotated to the position *trans* to the iron hydride in **3**. For the simplified structural model (isopropyl replaced with methyl), the calculated free energy of **3** is 5.8 kcal/mol higher than that of separated **2** and acetophenone. The following transition state [$\mathbf{TS}_{3,4}$ (Figure 2)] for the insertion of acetophenone into the Fe−H bond and the formation of a pentacoordinated alkoxo carbonyl complex **4** is 19.7 kcal/mol above **2**. Although the formation of **3** is indispensable for the insertion of acetophenone into the Fe−H bond and the following hydrogenation reaction, the formation of **3′** (Figure 2) through direct addition of an acetophenone molecule to **2** at the vacant position *trans* to the iron hydride was not considered in Milstein's mechanism. Calculation results indicate that **3′** is actually 8.8 kcal/mol more stable than **3** and 22.7 kcal/mol lower than $\mathbf{TS}_{3,4}$. To examine the steric effect, the structures of **3** and **3′** with the experimental isopropyl groups (**3**-^{i}**Pr** and **3′**-^{i}**Pr**, respectively) were also optimized and are displayed in Figure 2. It is obvious that the acetophenone ligands in **3**, **3′**, **3**-^{i}**Pr**, **3′**-^{i}**Pr**, and $\mathbf{TS}_{3,4}$ are far from the phosphorus methyl/isopropyl groups and have only very weak interactions between them. Therefore, the steric effect of isopropyl groups may slightly change the relative energies but will not change the conclusion that the acetophenone ligand is preferred for coordination of the vacant position *cis* to the nitrogen in **2** for the formation of **3′**. This is also confirmed by the calculated relative electronic energy of **3′**-^{i}**Pr**, which is 10.1 kcal/mol lower than that of **3**-^{i}**Pr**.

Instead of acetophenone, if a solvent EtOH molecule fills the vacant position in **2** and forms a slightly more stable intermediate, $\mathbf{2}_{EtOH}$, the O−H bond in EtOH can easily be split through transition state $\mathbf{TS}_{2,6}$ (Figure 2; $\Delta G^{\ddagger}$ = 15.5 kcal/mol) for the rearomatization of the pyridine ring and the formation of a much more stable intermediate **6**. The energy barrier of the reverse reaction (**6** → $\mathbf{TS}_{2,6}$) is only 16.4 kcal/mol. Therefore, **2** is stabilized by the reversible addition of EtOH. Because $\mathbf{TS}_{2,6}$ is 14.9 kcal/mol lower than $\mathbf{TS}_{3,4}$ and only 6.3 kcal/mol higher than $\mathbf{2}_{EtOH}$, the insertion of ketones into the Fe−H bond is very unlikely to happen because of the quick formation of **6** and the 31.3 kcal/mol free energy barrier between **6** and $\mathbf{TS}_{3,4}$.

If a dihydrogen molecule fills the vacant position in **2** (blue), the H_2 in intermediate $\mathbf{2}_{H_2}$ can easily be split by transferring a proton to the unsaturated carbon in the pincer ligand for the formation of the *trans* dihydride complex **7** with a free energy barrier of 16.6 kcal/mol ($\mathbf{2}_{H_2}$ → $\mathbf{TS}_{2,7}$). After comparing all relative energies shown in Figure 1 and considering the easy formation of **7**, we can conclude that the total free energy barrier for the insertion of acetophenone into the Fe−H bond is 40.8 kcal/mol (**7** → $\mathbf{TS}_{3,4}$), which is far too high to account for the observed catalytic reaction.

In addition, Milstein and co-workers observed a rapid reaction between [(PNP^{-H})FeH(CO)$(OCPh_2)$] ($\mathbf{2}_{OCPh_2}$) and H_2 generates **7** and a hydrido alkoxo complex [(PNP)FeH-(CO)$(OCHPh_2)$] ($\mathbf{5}_{OCHPh_2}$), but a very slow reaction between [(PNP^{-H})FeH(CO)(NCPh)] ($\mathbf{2}_{NCPh}$) and H_2 generates **7** only.[4] To understand why $\mathbf{2}_{OCPh_2}$ and $\mathbf{2}_{NCPh}$ have very different reactivities with H_2, the relative energies of $\mathbf{2}_{OCPh_2}$ and $\mathbf{2}_{NCPh}$ were also calculated. As shown in Figure 1, $\mathbf{2}_{OCPh_2}$ and $\mathbf{2}_{NCPh}$ are 4.8 and 8.7 kcal/mol more stable than **2**, respectively. Therefore, $\mathbf{TS}_{2,7}$ is 19.7 and 23.6 kcal/mol higher than $\mathbf{2}_{OCPh_2}$ and $\mathbf{2}_{NCPh}$, respectively. Such an energy barrier difference explains why the reaction between $\mathbf{2}_{OCPh_2}$ and H_2 is much faster than the reaction between $\mathbf{2}_{NCPh}$ and H_2.

Formation of 7 Catalyzed by EtOH. As shown in Scheme 2 and Figure 3, once **6** is formed through EtOH addition and O−H bond splitting, the dissociation of EtO^- anion from **6** in the ethanol solvent needs only 15.6 kcal/mol of free energy, which indicates a rapid H_2−EtO^- exchange for the formation of cationic intermediate **9**. Then an EtO^- approaches **9** again, takes a proton from the dihydrogen, and regenerates EtOH through transition state $\mathbf{TS}_{9,10}$. The newly formed EtOH molecule attaches to the iron center in **10** through a weak Fe−

dx.doi.org/10.1021/ic2020176 | *Inorg. Chem.* 2011, 50, 12836–12843

Scheme 2. Predicted Mechanism for Formation of 7 Catalyzed by EtOH

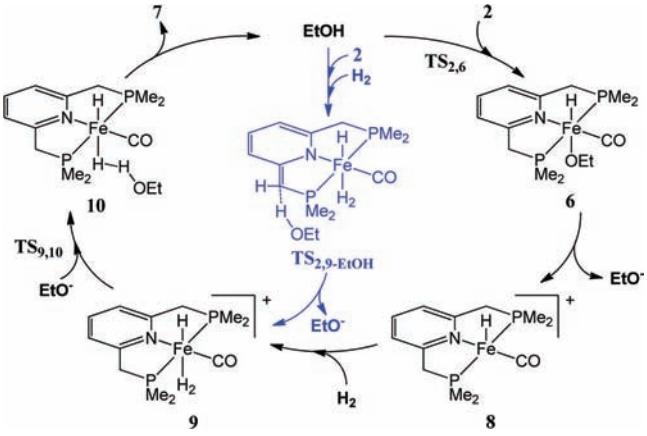

$H^{\delta-}\cdots H^{\delta+}$–O dihydrogen bond with a $H^{\delta-}\cdots H^{\delta+}$ distance of 1.681 Å. The dissociation of EtOH from **10** is a 5.2 kcal/mol downhill step. Because $\mathbf{TS}_{2,6}$ is 10.1 kcal/mol lower than $\mathbf{TS}_{2,7}$, the formation of **6** is much faster than the direct formation of **7** from $\mathbf{2}_{H_2}$. The formation of **7** therefore primarily follows the EtOH-catalyzed reaction pathway shown in Scheme 2 (black) with a total energy barrier of 17.2 kcal/mol (**6** → $\mathbf{TS}_{9,10}$). Such results indicate that the essential role of solvent ethanol in the whole reaction is not only to stabilize dearomatized **2** but also more importantly to catalyze the formation of **7**.

In addition to the direct H_2 cleavage in $\mathbf{2}_{H_2}$ and EtOH-catalyzed H_2 splitting for the formation of **7** described above, the possibility of H_2 splitting and CH_2 formation through proton transfer in $\mathbf{2}_{H_2}$ mediated by a solvent EtOH molecule was also explored (Scheme 2 and Figure 3, blue route). Although an EtOH molecule can attach to $\mathbf{2}_{H_2}$ and form an unstable $\mathbf{2}_{H_2\text{-EtOH}}$ intermediate (Figure 4), all attempts to locate a transition state transferring two protons simultaneously for the cleavage of H_2 and the formation of CH_2 bridged by the ethanol oxygen failed. However, once $\mathbf{2}_{H_2\text{-EtOH}}$ is formed, a proton on the oxygen in EtOH can be transferred to the unsaturated carbon in the pincer ligand through transition state $\mathbf{TS}_{2,9\text{-EtOH}}$ (Figure 4; $\Delta G^{\ddagger}$ = 6.9 kcal/mol) for the formation of a rearomatized intermediate $\mathbf{9}_{EtO}$ (ΔG° = 4.3 kcal/mol). The dissociation of EtO^- from $\mathbf{9}_{EtO}$ in the ethanol solvent is a 3.7 kcal/mol downhill step. Therefore, the cleavage of H_2 and the formation of **7** through proton transfer mediated by a solvent EtOH molecule contain at least two elementary steps, O–H bond cleavage and H_2 splitting, which cannot be accomplished through only one transition state. Because $\mathbf{TS}_{2,9\text{-EtOH}}$ is only 1.3 and 2.1 kcal/mol higher than $\mathbf{TS}_{9,10}$ and $\mathbf{TS}_{2,6}$, respectively, the two routes shown in Scheme 2 and Figure 3 for the formation of **7** are competitive.

Hydrogenation of Acetophenone Catalyzed by 7. A direct reduction mechanism for the hydrogenation of acetophenone catalyzed by **7** is proposed and shown in Scheme 3 and Figure 5. There are three reaction pathways (black, blue, and red) starting with direct transfer of hydride from Fe to the unsaturated carbon in acetophenone **7** for the formation of an unstable intermediate **11** with a free energy barrier of 17.1 kcal/mol [$\mathbf{TS}_{7,11}$ (Figure 6)]. The dissociation of $PhMeCHO^-$ from **11** for the generation of monocation **8** in the ethanol solvent is an only 3.0 kcal/mol uphill step. Similarly, the formation of Ph_2CHO^- in the reaction of **2** with benzophenone and H_2 was observed by Milstein and co-workers (experimental details given in the Supporting Information of ref 4). Such observation further confirms the easy dissociation of the $PhMeCHO^-$ and **8** ion pair in the solvent. Depending on which ligand (H_2 or $PhMeCHO^-$) fills the vacant position in **8**, there are two reaction pathways for the production of 1-phenylethanol and regeneration of **7**.

In the first pathway (black in Scheme 3 and Figure 5), a H_2 molecule fills the vacant position in **8** and forms a slightly more stable cationic intermediate **9**. Then a $PhMeCHO^-$ approaches the dihydrogen in **9** and forms 1-phenylethanol by taking a proton from H_2 through transition state $\mathbf{TS}_{9,12}$ (Figure 6), which is only 2.8 kcal/mol higher in free energy than **9**. H_2 cleavage product **12** has a weak $Fe{-}H^{\delta-}\cdots H^{\delta+}{-}O$ dihydrogen bond connecting the newly formed 1-phenylethanol and the iron center with a H···H distance of 1.657 Å. The dissociation of 1-phenylethanol from **12** for the regeneration of **7** is a 3.4 kcal/mol downhill step.

The second pathway (blue in Schem 3 and Figure 5) begins with the reassociation of $PhMeCHO^-$ and **8**, which forms a stable intermediate **5** with an Fe–O distance of 2.029 Å. **5** is 16.8 kcal/mol more stable than **11** and should be considered as the resting state in this catalytic reaction. Because **5** and **7** have very close relative free energies, they may exist together in the reaction with a low H_2 pressure. This is in agreement with the

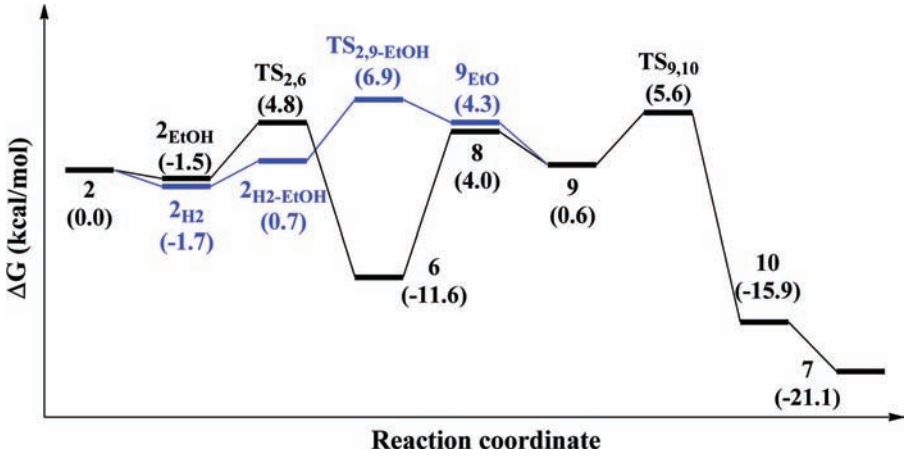

Figure 3. Free energy profile for the formation of **7** catalyzed by EtOH.

dx.doi.org/10.1021/ic2020176 | *Inorg. Chem.* 2011, 50, 12836–12843

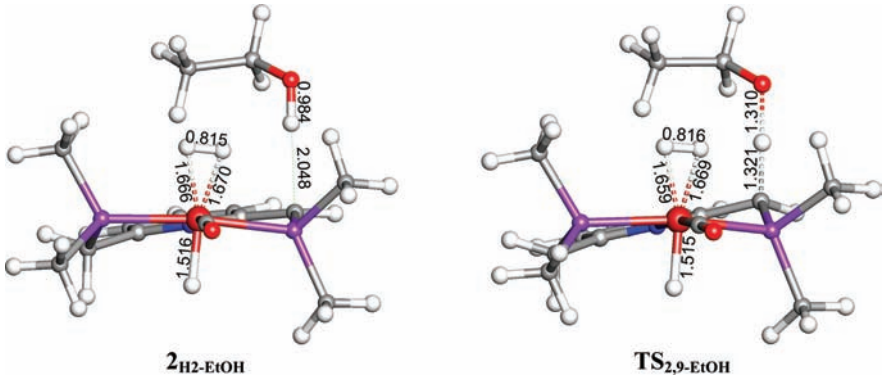

Figure 4. Optimized structures of $\mathbf{2}_{H_2\text{-}EtOH}$ and $\mathbf{TS}_{2,9\text{-}EtOH}$ ($1271i$ cm^{-1}) in the reaction pathway of H_2 cleavage catalyzed by EtOH. Bond lengths are in angstroms.

Scheme 3. Direct Reduction Mechanism for the Hydrogenation of Acetophenone Catalyzed by 7

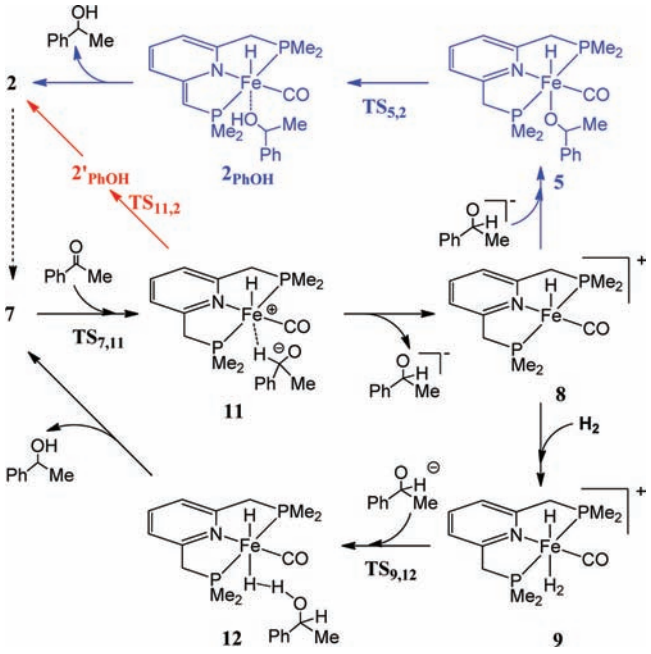

formation of a similar hydrido alkoxo complex $\mathbf{5}_{OCHPh_2}$ together with **7** in the reaction of **2** with benzophenone and 1 atm of H_2 observed by Milstein and co-workers.[4] The $PhMeCHO^-$ ligand in **5** can easily catch a methylene proton in the PNP ligand and form 1-phenylethanol through transition state $\mathbf{TS}_{5,2}$. The dissociation of 1-phenylethanol from $\mathbf{2}_{PhOH}$ for the regeneration of **2** is only 3.7 kcal/mol uphill in the ethanol solvent. Then **7** can be regenerated with the assistance of the solvent EtOH through the reaction pathways shown in Scheme 2. Because of the formation of **5** and the barrier for the regeneration of **7**, the total free energy barrier of this route ($\mathbf{5} \rightarrow \mathbf{TS}_{9,10}$) is 22.2 kcal/mol, which can be achieved under mild condition but is 2.4 kcal/mol less favorable than the direct H_2 cleavage pathway.

In addition, the possibility that **7** simultaneously transfers a hydride from Fe to the acetophenone carbon and transfers a proton from a CH_2 to the acetophenone oxygen was also examined (red in Schems 3 and Figure 5). All attempts to locate such a bifuntional transition state for the direct generation of 1-phenylethanol and **2** failed. However, after **11** is formed by the transfer of a hydride from Fe to the acetophenone carbon, a methylene proton can be transferred to the acetophenone oxygen through transition state $\mathbf{TS}_{11,2}$ (Figure 6; $\Delta G^{\ddagger}$ = 10.2 kcal/mol) for the formation of 1-phenylethanol. The newly formed unstable intermediate $\mathbf{2'}_{PhOH}$ is a 4.4 kcal/mol less stable isomer of $\mathbf{2}_{PhOH}$. Therefore, such direct formation of 1-phenylethanol from **7** by transfer of an

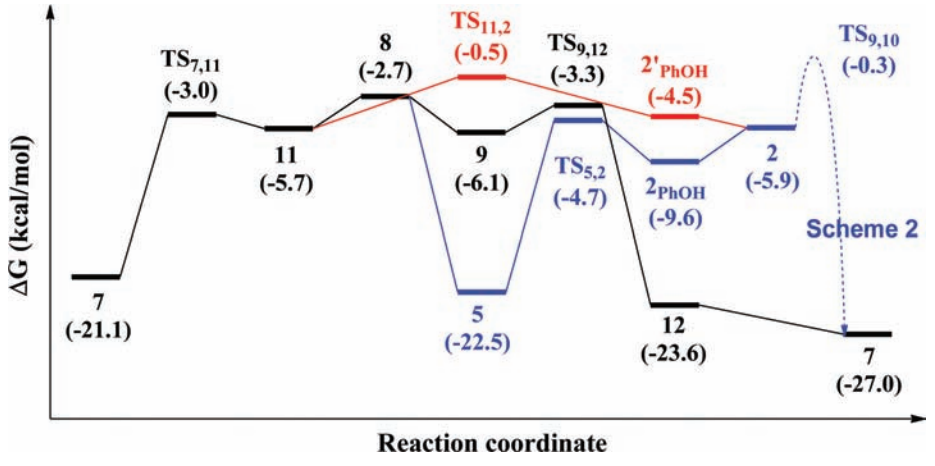

Figure 5. Calculated relative free energies of the intermediates and transition states in the direct reduction mechanism for the hydrogenation of acetophenone catalyzed by **7**.

dx.doi.org/10.1021/ic2020176 | *Inorg. Chem.* 2011, 50, 12836–12843

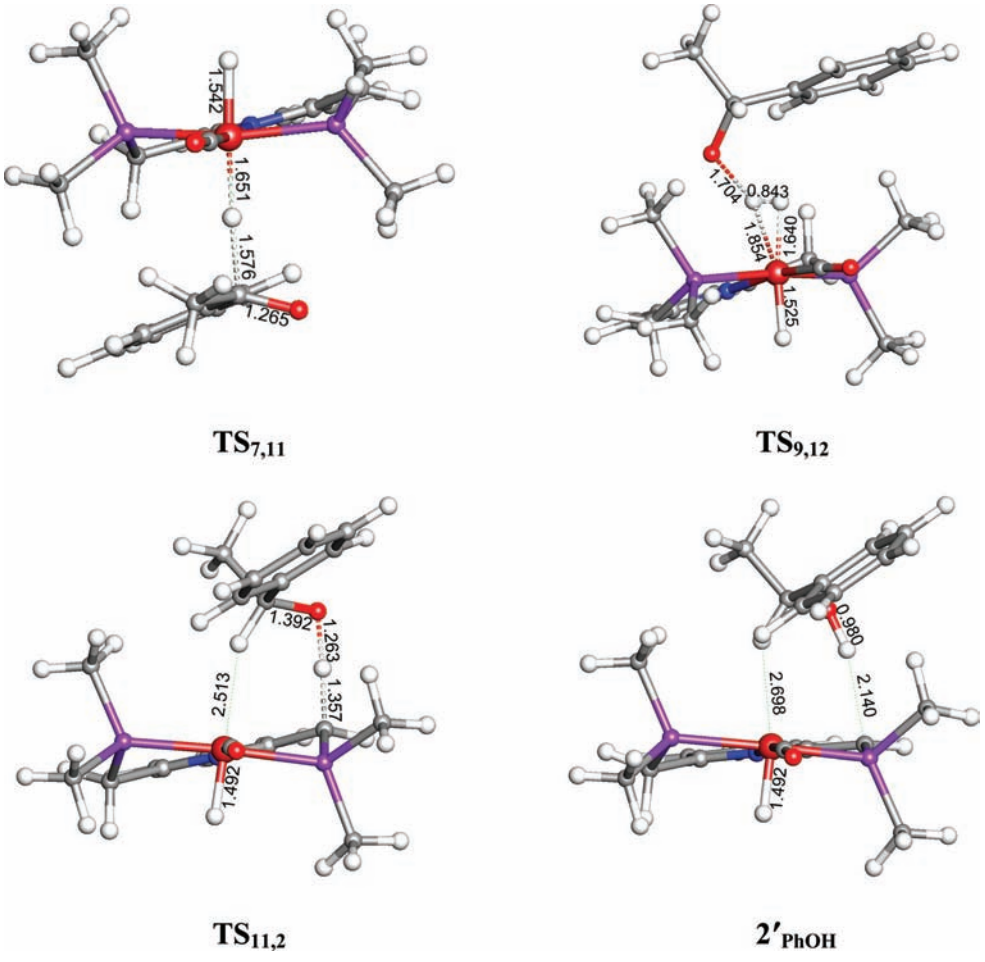

Figure 6. Optimized structures of $\mathbf{TS}_{7,11}$ (607*i* cm^{-1}), $\mathbf{TS}_{9,12}$ (199*i* cm^{-1}), $\mathbf{TS}_{11,2}$ (1357*i* cm^{-1}), and $\mathbf{2}'_{PhOH}$. Bond lengths are in angstroms.

iron hydride and a methylene proton to acetophenone contains at least two elementary steps and cannot be accomplished through only one transition state. Because $\mathbf{TS}_{11,2}$ is 0.2 kcal/mol lower than $\mathbf{TS}_{9,10}$ and 2.2 kcal/mol higher than **8**, this consecutive metal hydride and ligand proton transfer pathway for the hydrogenation of acetophenone is also accessible under mild conditions but less favorable than the direct H_2 cleavage pathway described above.

■ CONCLUSIONS

In summary, the hydrogenation of acetophenone catalyzed by iron PNP pincer complexes was studied using density functional theory with the proposal of an unexpected direction reduction mechanism. The essential role of the alcoholic solvent in the whole hydrogenation reaction is not only a stabilizer of the dearomatized intermediate **2** but also more importantly an assistant catalyst for the formation of stable *trans* dihydride complex **7**, which is the actual ketone hydrogenation catalyst. Because of the quick formation of **7** catalyzed by EtOH, the calculated total free energy barrier using a simplified structural model for the hydrogenation of acetophenone in the catalytic cycle proposed by Milstein and co-workers is 40.8 kcal/mol (**7** → $\mathbf{TS}_{3,4}$), which is therefore far too high to account for the observed catalytic reaction.

A direct reduction mechanism, which features direct transfer of hydride to the acetophenone carbon from the catalyst and H_2 cleavage by hydrido alkoxo without the participation of the PNP pincer ligand, was proposed on the basis of calculation results. The turnover-limiting step in this catalytic reaction is the $PhMeCHO^{-}-H_2$ exchange in **5** for the formation of **9**. A higher H_2 pressure will accelerate the reaction by generating a higher percentage of **9** for further reaction. The total free energy barrier of this newly proposed mechanism for the simplified structural model is only 19.8 kcal/mol (**5** → **8**), which leads to a reaction rate of 68 h^{-1} at standard state and 298.15 K using the transition state theory. The energetics would be slightly different if the experimental structure could be calculated. The newly proposed mechanism also suggests that the incorporation of a strong base, proper alcohols, and unsaturated ligands may be critical for the design of high-efficiency and low-cost catalysts for hydrogen activation and hydrogenation of ketones.

■ COMPUTATIONAL DETAILS

All DFT calculations were performed using the Gaussian 09 suite of ab initio programs[7] at the range-separated and dispersion-corrected hybrid functional ωB97X-D[8] in conjunction with the all-electron 6-31++G(d,p) basis set[9] for all atom levels of theory. We believe such basis sets (for example, 678 basis functions and 1197 primitive Gaussians for **5**) used in our study are sufficient for accurate DFT calculations. The ωB97X-D functional was selected for this study because it includes both long-range exchange and empirical dispersion corrections, which are very important for the modeling of processes with weak interactions and localized anionic or strongly electron donating sites.[10] The ωB97X-D functional was recently examined by Hall and co-workers as one of the most encouraging functionals for the study of kinetic barriers in an addition of ethylene to nickel

dx.doi.org/10.1021/ic2020176 | *Inorg. Chem.* 2011, 50, 12836–12843

bis(dithiolene).[11] Isopropyl groups were replaced with methyl groups in all calculated metal complexes to reduce the cost of computational resources without a significant degradation in the accuracy of predicted energy barriers. Detailed evaluation of such a simplified structural model is provided in the following section with the calculations of the relative energies between several key intermediates and transition states using the experimental structures. Calculation results indicate that the difference in the steric effects between the isopropyl and methyl groups in these metal pincer complexes is trivial and negligible.

All structures studied in this paper were fully optimized with solvent corrections using the integral equation formalism polarizable continuum model (IEFPCM)[12] with SMD[13] atomic radii for ethanol. An ultrafine integration grid (99590) was used for numerical integrations. The ground states of intermediates were confirmed as singlets through comparison with the optimized high-spin analogues. Because most of the experimental catalytic hydrogenation reactions occur at room temperature, thermal corrections were calculated within the harmonic potential approximation on optimized structures at 298.15 K and 1 atm. Unless otherwise noted, the energies reported in the text are solvent-corrected free energies. Calculating the harmonic vibrational frequencies for optimized structures and noting the number of imaginary frequencies (IFs) confirmed the nature of all intermediates (no IF) and transition state structures (only one IF). The latter were also confirmed to connect reactants and products by intrinsic reaction coordinate (IRC) calculations. The three-dimensional molecular structure figures displayed in this paper were drawn by using the *JIMP2* molecular visualizing and manipulating program.[14]

EVALUATION OF THE STRUCTURAL MODEL

To evaluate the steric effect of isopropyl groups and validate the reliability of the simplified structural model in the computational study, we fully optimized the relative energies of several key intermediate and transition state structures with experimental isopropyl groups in the proton transfer ($\mathbf{5} \rightarrow \mathbf{TS}_{5,2}$) and H_2 cleavage ($\mathbf{2}_{H_2} \rightarrow \mathbf{TS}_{2,7}$) reactions using the same method mentioned in Computational Details. As shown in Table 1, the changes in relative electronic energies caused by the use of a simplified model are less than 0.5 kcal/mol in these key steps. Therefore, the difference in steric effects between the isopropyl and methyl groups in these metal complexes is trivial and negligible. The reliability of the simplified structural model for computational reaction kinetics study is therefore well validated.

Table 1. Relative Electronic Energies of O−H Bond Formation ($\mathbf{5} \rightarrow \mathbf{TS}_{5,2}$) and H_2 Cleavage ($\mathbf{2}_{H_2} \rightarrow \mathbf{TS}_{2,7}$) Reactions for the Structures Using the Experimental Isopropyl Groups and the Methyl Substituents

	relative electronic energy (kcal/mol)	
ligand	$E^{\ddagger}(\mathbf{TS}_{5,2}) - E^{\circ}(\mathbf{5})$	$E^{\ddagger}(\mathbf{TS}_{2,7}) - E^{\circ}(\mathbf{2}_{H_2})$
isopropyl	20.44	18.62
methyl	20.05	18.37

EVALUATION OF DENSITY FUNCTIONALS

To examine the effect of different density functionals on the calculated energy barriers in this transition metal system, we selected nine other well-known or recently developed density functionals, including pure density functionals TPSS[15] and M06L[16] and hybrid density functionals TPSSh,[15] M06,[16] B3LYP,[17] B3PW91,[18] BMK,[19] HSE06,[20] and LC-ωPBE,[21] to calculate the electronic energy barriers of two key steps, $\mathbf{5} \rightarrow \mathbf{TS}_{5,2}$ and $\mathbf{2}_{H_2} \rightarrow \mathbf{TS}_{2,7}$, using the same basis set at ωB97X-D-optimized structures. As shown in Table 2, the difference in calculated relative electronic energies using these 10 density functionals is less than 4 kcal/mol for the $\mathbf{5} \rightarrow \mathbf{TS}_{5,2}$ step and less than 5 kcal/mol for the $\mathbf{2}_{H_2} \rightarrow \mathbf{TS}_{2,7}$ step. The ωB97X-D results are between those two values. It is obvious that the chemical conclusions in this study are generally independent of the functional chosen. More importantly, the estimated reaction rate of 68 h^{-1} at standard state and 298.15 K using the ωB97X-D calculated total free energy barrier of 19.8 kcal/mol is very close to the observed TOF of 87 h^{-1} at room temperature and 4.1 atm of H_2. Therefore, ωB97X-D is a reliable functional for the study of this iron-catalyzed ketone hydrogenation system.

Table 2. Relative Electronic Energies of O−H Bond Formation ($\mathbf{5} \rightarrow \mathbf{TS}_{5,2}$) and H_2 Cleavage ($\mathbf{2}_{H_2} \rightarrow \mathbf{TS}_{2,7}$) Reactions Obtained Using Different Density Functionals for ωB97X-D-Optimized Structures

	relative electronic energy (kcal/mol)	
density functional	$E^{\ddagger}(\mathbf{TS}_{5,2}) - E^{\circ}(\mathbf{5})$	$E^{\ddagger}(\mathbf{TS}_{2,7}) - E^{\circ}(\mathbf{2}_{H_2})$
ωB97X-D	20.05	18.37
TPSS	18.32	15.21
M06L	20.80	15.88
TPSSh	18.90	16.08
M06	20.36	17.69
B3LYP	20.16	17.99
B3PW91	17.62	16.85
BMK	21.56	16.95
HSE06	17.81	16.99
LC-ωPBE	19.98	20.06

ASSOCIATED CONTENT

Supporting Information

Computational details, complete ref 7, solvent corrected absolute free energies, and atomic coordinates of optimized structures. This material is available free of charge via the Internet at http://pubs.acs.org.

AUTHOR INFORMATION

Corresponding Author

*E-mail: yangxz@berkeley.edu; yangxinzheng@gmail.com.

ACKNOWLEDGMENTS

This work was supported by the Molecular Graphics and Computation Facility (Dr. Kathleen A. Durkin, Director) in the College of Chemistry at the University of California (Berkeley, CA) and by the National Science Foundation (Grant CHE-0840505 for the computational devices). I appreciate constructive discussion with Dr. Jian Yang (University of California, Berkeley, CA).

REFERENCES

(1) de Vries, J. G., Elsevier, C. J., Eds. *Handbook of Homogeneous Hydrogenation*; Wiley-VCH: Weinheim, Germany, 2007; Vol. *1*, Chapter 37.

(2) (a) Malacea, R.; Poli, R.; Manoury, E. *Coord. Chem. Rev.* **2010**, *254*, 729. (b) Matsumura, K.; Arai, N.; Hori, K.; Saito, T.; Sayo, N.; Ohkuma, T. *J. Am. Chem. Soc.* **2011**, *133*, 10696. (c) Lundberg, H.; Adolfsson, H. *Tetrahedron Lett.* **2011**, *52*, 2754. (d) Noyori, R. *Angew. Chem., Int. Ed.* **2002**, *41*, 2008. (e) Noyori, R.; Hashiguchi, S. *Acc. Chem. Res.* **1997**, *30*, 97.

(3) (a) Morris, R. H. *Chem. Soc. Rev.* **2009**, *38*, 2282. (b) Casey, C. P.; Guan, H. *J. Am. Chem. Soc.* **2007**, *129*, 5816. (c) Junge, K.; Wendt, B.; Addis, D.; Zhou, S.; Das, S.; Fleischer, S.; Beller, M. *Chem.—Eur. J.* **2011**, *17*, 101. (d) Bauer, G.; Kirchner, K. A. *Angew. Chem., Int. Ed.* **2011**, *50*, 5798. (e) Lagaditis, P. O.; Lough, A. J.; Morris, R. H. *J. Am. Chem. Soc.* **2011**, *133*, 9662. (f) Chen, H.-Y. T.; Tommaso, D. D.; Hogarth, G.; Catlowa, C. R. A. *Dalton Trans.* **2011**, *40*, 402. (g) Chen, Y.; Tang, Y.; Lei, M. *Dalton Trans.* **2009**, 2359.

(4) Langer, R.; Leitus, G.; Ben-David, Y.; Milstein, D. *Angew. Chem., Int. Ed.* **2011**, *50*, 2120.
(5) Yang, X. *ACS Catal.* **2011**, *1*, 849.
(6) Langer, R.; Diskin-Posner, Y.; Leitus, G.; Shimon, L. J. W.; Ben-David, Y.; Milstein, D. *Angew. Chem., Int. Ed.* **2011**, *50*, 9948.
(7) Frisch, M. J.; et al. *Gaussian 09*, revision B.01; Gaussian, Inc.: Wallingford, CT, 2010.
(8) Chai, J.-D.; Head-Gordon, M. *Phys. Chem. Chem. Phys.* **2008**, *10*, 6615.
(9) (a) Hehre, W. J.; Ditchfield, R.; Pople, J. A. *J. Chem. Phys.* **1972**, *56*, 2257. (b) Hariharan, P. C.; Pople, J. A. *Theor. Chim. Acta* **1973**, *28*, 213. (c) Krishnan, R.; Binkley, J. S.; Seeger, R.; Pople, J. A. *J. Chem. Phys.* **1980**, *72*, 650.
(10) (a) Jensen, F. *J. Chem. Theory Comput.* **2010**, *6*, 2726. (b) Thanthiriwatte, K. S.; Hohenstein, E. G.; Burns, L. A.; Sherrill, C. D. *J. Chem. Theory Comput.* **2011**, *7*, 88.
(11) Dang, L.; Yang, X.; Brothers, E. N.; Hall, M. B. *J. Phys. Chem. A* **2012**, in press. DOI: 10.1021/jp205971b.
(12) Tomasi, J.; Mennucci, B.; Cammi, R. *Chem. Rev.* **2005**, *105*, 2999.
(13) Marenich, A. V.; Cramer, C. J.; Truhlar, D. G. *J. Phys. Chem. B* **2009**, *113*, 6378.
(14) Manson, J.; Webster, C. E.; Hall, M. B. *JIMP2, version 0.091, a free program for visualizing and manipulating molecules*; Texas A&M University: College Station, TX, 2006.
(15) Tao, J. M.; Perdew, J. P.; Staroverov, V. N.; Scuseria, G. E. *Phys. Rev. Lett.* **2003**, *91*, 146401.
(16) Zhao, Y.; Truhlar, D. G. *Theor. Chem. Acc.* **2008**, *120*, 215.
(17) (a) Becke, A. D. *J. Chem. Phys.* **1993**, *98*, 5648. (b) Lee, C.; Yang, W.; Parr, R. G. *Phys. Rev. B* **1988**, *37*, 785.
(18) (a) Burke, K.; Perdew, J. P.; Wang, Y. In *Electronic Density Functional Theory: Recent Progress and New Directions*; Dobson, J. F., Vignale, G., Das, M. P., Eds.; Plenum: New York, 1998. (b) Perdew, J. P. In *Electronic Structure of Solids '91*; Ziesche, P., Eschrig, H., Eds.; Akademie Verlag: Berlin, 1991. (c) Perdew, J. P.; Chevary, J. A.; Vosko, S. H.; Jackson, K. A.; Pederson, M. R.; Singh, D. J.; Fiolhais, C. *Phys. Rev. B* **1992**, *46*, 6671. (d) Perdew, J. P.; Chevary, J. A.; Vosko, S. H.; Jackson, K. A.; Pederson, M. R.; Singh, D. J.; Fiolhais, C. *Phys. Rev. B* **1993**, *48*, 4978. (e) Perdew, J. P.; Burke, K.; Wang, Y. *Phys. Rev. B* **1996**, *54*, 16533.
(19) Boese, A. D.; Martin, J. M. L. *J. Chem. Phys.* **2004**, *121*, 3405.
(20) (a) Henderson, T. M.; Izmaylov, A. F.; Scalmani, G.; Scuseria, G. E. *J. Chem. Phys.* **2009**, *131*, 044108. (b) Krukau, A. V.; Vydrov, O. A.; Izmaylov, A. F.; Scuseria, G. E. *J. Chem. Phys.* **2006**, *125*, 224106.
(21) (a) Vydrov, O. A.; Scuseria, G. E.; Perdew, J. P. *J. Chem. Phys.* **2007**, *126*, 154109. (b) Vydrov, O. A.; Scuseria, G. E. *J. Chem. Phys.* **2006**, *125*, 234109.